Fusion Engineering and Design 187 (2023) 113378

Contents lists available at ScienceDirect

Fusion Engineering and Design

journal homepage: www.elsevier.com/locate/fusengdes

Toroidal magnetic field ripple in the presence of misaligned toroidal field coils on the COMPASS-U tokamak

Lukas Kripner [a,b,*], Jaroslav Krbec [a], Jan Zelda [a], Tomas Markovic [a,b], Peter Titus [c], Petr Vondracek [a], Ondrej Ficker [a], Martin Hron [a]

[a] Institute of Plasma Physics of the CAS, U Slovanky 1770/3, Prague, 182 00, Czech Republic
[b] Faculty of Mathematics and Physics, Charles University, V Holesovickach 2, Prague, 180 00, Czech Republic
[c] Princeton Plasma Physics Laboratory, 100 Stellarator Rd, Princeton, 085 40, NJ, USA

ARTICLE INFO

Keywords:
Tokamak
Toroidal field ripple
Toroidal magnetic field coils
ANSYS

ABSTRACT

Homogeneity of the toroidal magnetic field is a critical aspect of the tokamak fusion device. It is affected by the design of toroidal magnetic field coils and their manufacturing and assembly misalignments. The magnetic field of the COMPASS-U project is analysed using toroidal field ripple quantity. ANSYS modelling of bitter-plate-designed toroidal field coils is performed to prepare an accurate simplistic representation of the coils using a virtual current line. Toroidal field ripple is analysed using a Gaussian distribution of possible misalignments. The worst-case toroidal field ripple corresponding to the technical drawings only slightly exceeds the chosen limit of 0.5%.

1. Introduction

A new medium size tokamak COMPASS Upgrade (COMPASS-U) [1,2] with high magnetic field and high-density plasma ($R = 0.9\,\mathrm{m}$, $B_t = 5\,\mathrm{T}$, $I_p = 2\,\mathrm{MA}$, $n_e \approx 10^{20}\,\mathrm{m}^{-3}$) is being designed and under construction at the Institute of Plasma Physics in Prague. With its parameters and rich diagnostics coverage, it has the potential to address the challenges in advanced plasma confinement modes and configurations and plasma exhaust physics. The machine contribution is also expected in new plasma-facing materials testing and design concepts.

Toroidal field ripple

In this article, we analyse inhomogeneities of toroidal magnetic field using the *toroidal field ripple* quantity defined as [3,4]

$$\delta(R,Z) = \frac{\max_\phi |B| - \min_\phi |B|}{\max_\phi |B| + \min_\phi |B|} \cdot 100\%, \tag{1}$$

where the minimum and maximum of the magnetic field magnitude are calculated over all toroidal angles ϕ for a given poloidal position.

In some previous works, the toroidal field ripple is calculated only from the toroidal component of the magnetic field [5]. However, since these works do not evaluate misalignments which are caused by other than the toroidal component of the magnetic field and the fact that the toroidal field component is dominant, both definitions can be mutually compared. Therefore, we decided to use the definition which is using the total magnetic field magnitude due to the nature of the ripple consequences.

The magnitude of the maximal toroidal field ripple typically varies from 0.08% for JET [3] through $\delta \sim 0.66\%$ for ASDEX Upgrade [6] to 3% for JT60-U [7]. Design target value for COMPASS-U was chosen to be $\delta < 0.5\%$. This value corresponds to the ripple value on ITER $\delta \sim 0.5\%$ [3].

The toroidal field ripple may have various effects on plasma performance [3,4,8–10]. For example, plasma rotation breaking or fast ion losses are among the well-known and relevant for COMPASS-U. Therefore, the restrictions originating from the toroidal field ripple are essential for toroidal field (TF) coil design.

Aside from the toroidal field ripple, the magnetic coil winding and its misalignments are causing so-called error fields, affecting the MHD stability of the plasma [11,12]. The proper evaluation of the error field requires a calculation of the plasma response [13]. However, the evaluation of the error fields for COMPASS-U is not the subject of this paper.

Ripple loss mechanism. Ref. [4] describes three types of ripple-induced fast ion losses. First, *ripple trapping*, which is affected mainly by the toroidal field ripple along the tokamak midplane. Second, the magnitude of the ion loss caused by the *stochastic ripple diffusion* mechanism is influenced by the toroidal field ripple in the vicinity of the plasma

* Corresponding author at: Institute of Plasma Physics of the CAS, U Slovanky 1770/3, Prague, 182 00, Czech Republic.
E-mail address: kripner@ipp.cas.cz (L. Kripner).

https://doi.org/10.1016/j.fusengdes.2022.113378
Received 11 July 2022; Received in revised form 6 December 2022; Accepted 9 December 2022
Available online 19 December 2022

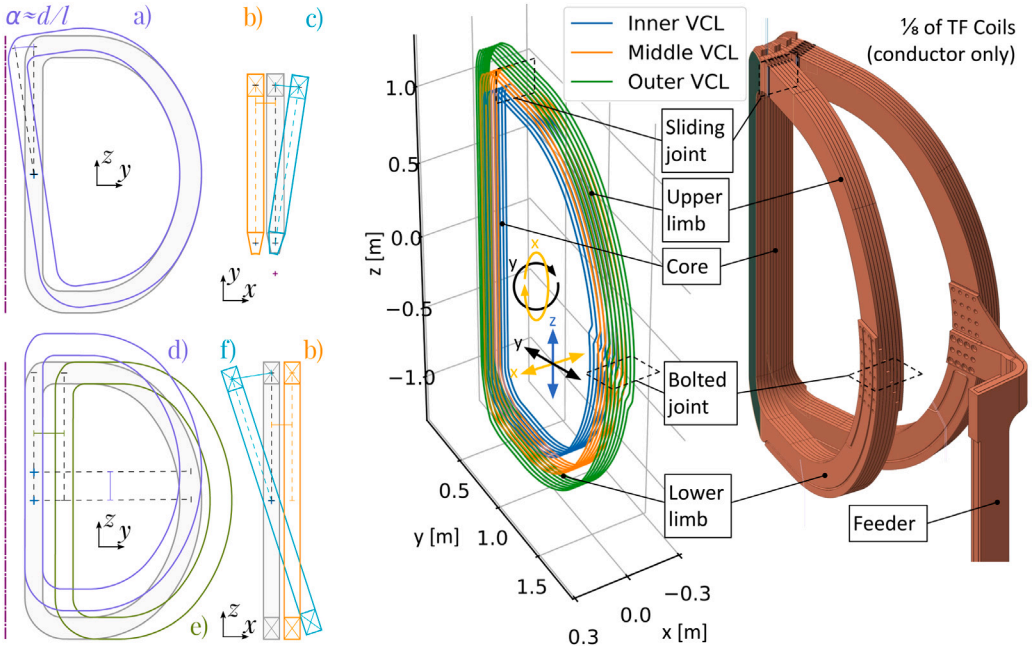

Fig. 1. (left) Schematics of all considered displacements: (a) in-plane tilt, (b) normal shift, (c) axis tilt, (d) vertical shift, (e) radial shift, and (f) out-of-plane tilt. (right) Realistic CAD drawing of winding of 1/8 of whole TF coils structure and virtual current lines used for magnetic field calculations. All coils are supplied by one feeder line.

separatrix. Finally, *collisional ripple diffusion* is considered the weakest loss mechanism.

In this article, we first describe the current design of TF coils. In the next section, the methodology of toroidal field ripple calculations is explained. The results section shows the current distribution in the perfectly aligned coil mass during the discharge sequence and discusses its impact on the unperturbed toroidal field ripple. Next, we present the results of the analysis of the ripple caused by misaligned TF coils using the Monte Carlo technique. Finally, we provide the spectral analysis of the calculated ripple.

COMPASS-U magnetic coil system

COMPASS-U magnetic coil system is designed with 16 TF coils and 16 coils of poloidal field. The poloidal field coils are divided into the central solenoid (CS) coils, whose primary purpose is to induce the current through the plasma and poloidal field (PF) coils, whose primary purpose is to shape the plasma. The toroidal magnetic field generated by the TF coils is the strongest of the fields generated by the magnetic coils. TF coils have a bitter plate-like design (see Fig. 1(right)) with a toroidally continuous stack of copper plates and insulation in the core and 16 discrete bundles of seven insulated plates (20 mm × 200 mm). Turn-to-turn transition is created by a shift of the upper limb by one turn in overlapped bolted joint. All the coils are supplied by a single feeder connected at the bolted joint location. The sliding joint provides a straight conductor connection whose purpose is to mitigate the transfer of the structural loads between the core and upper limb. Each coil consists of two parts: upper limb and core with lower limb. The lower limb is connected with the upper limb by the midplane bolted join, while the core is connected with the upper limb with the sliding joint. This way, the turns form a continuous winding of all 16 coils. The coil is designed as ∼2.5 m height with ∼3.6 m in diameter and weight of ∼24 t.

Each coil consists of seven toroidally separated turns (plates) that house three virtual current lines (VCL) for electric current simulations (inner, middle and outer VCL). The accuracy of this representation is discussed in Section 3. We selected inner, middle and outer VCL as shown in Fig. 1. This model includes bolted joints as well as coil-to-coil transitions.

2. Methodology

The resulting effect of coil misalignment is calculated in the following manner. The detailed static magnetic field of the single VCL is calculated using Biot–Savart law in the form convenient for thin wire representation

$$\vec{B}(\vec{r}) = \frac{\mu_0 I}{4\pi} \int \frac{\mathrm{d}\vec{l} \times (\vec{r} - \vec{r})}{|\vec{r} - \vec{r}|^3}, \tag{2}$$

where $\mathrm{d}\vec{l}$ is the length element of the coil, μ_0 vacuum magnetic permeability and I is the current flowing through VCL. The usage of VCL is justified in Section 3. Biot–Savart law is calculated using the Biot–Savart integrators python package [14].

The resulting deviated magnetic field is calculated in the following manner. First, the magnetic field of the reference TF coil $\vec{B}_0(\vec{r})$ is calculated using Eq. (2) on the (R, ϕ, Z) grid. The reference coil is chosen to be aligned with the YZ plane. Second, an array of spatial points $\vec{r}$ where the field will be evaluated is chosen. In this article, we mainly use a grid of points distributed in the toroidal direction along the midplane, where the strongest toroidal field ripple is present (see Fig. 3). Third, deviated field of ith TF coil is evaluated by applying rotations or translations of the magnetic field.

The calculated misalignments can be divided into *tilts* and *shifts*. Shifts (translations) are evaluated fairly simply by

$$\vec{B}_{\mathrm{shift}}(\vec{r}) = \vec{B}_0(\vec{r} - \vec{T}), \tag{3}$$

where $\vec{T}$ represents the sum of applied translations. Clearly, the application of translation is commutative. Coil tilt is calculated as a rotation of the coil field with respect to the axis shifted from the origin.

$$\vec{B}_{\mathrm{tilt}}(\vec{r}) = \mathbf{R}\vec{B}_0(\mathbf{R}^{-1}(\vec{r} - \vec{A}) + \vec{A}), \tag{4}$$

where $\vec{A}$ is the position of the rotational axis and matrix $\mathbf{R}$ is the rotation matrix representing the resulting coil tilt. Since we rotate vectors $\vec{r}$, where the field is evaluated, first, the inverse rotation is applied, and consequently, the original rotation matrix is applied to field vectors to return them to the original coordinate system. As a result, the deviation field of ith coil, rotated by ϕ_i from the origin, can be calculated as

$$\vec{B}_{\mathrm{dev},i}(\vec{r}) = \mathbf{R}_{z,\phi_i}\mathbf{R}\vec{B}_0(\mathbf{R}^{-1}(\mathbf{R}^{-1}_{z,\phi_i}\vec{r} - \vec{A}) + \vec{A} - \vec{T}), \tag{5}$$

Table 1
Overview of considered misalignments, their maximal allowable deviations according to technical drawings of TF coils and rotation arm lengths.

Misalignment	Transformation	3σ [mm]	l [mm]
Normal shift	Translation in x	0.5	
Radial shift	Translation in y	0.5	
Vertical shift	Translation in z	0.1	
In-plane tilt	Rotation in x axis	1.5 (120″)	1.175
Out-of-plane tilt	Rotation in y axis	1.5 (120″)	1.175
Axis tilt	Rotation in z axis	1.1 (120″)	1.44

where $\mathbf{R}_{z,\phi_i}$ is a toroidal rotation of the coil to its position ϕ_i with respect to the referent TF coil. Finally, the field of all TF coils is summed up

$$\vec{B}_{\mathrm{dev}}(\vec{r}) = \sum_{i=1}^{16} \vec{B}_{\mathrm{dev},i}(\vec{r}). \tag{6}$$

This contribution analyses three types of shift: normal shift, radial shift and vertical shift, and three types of tilt: axis tilt, in-plane tilt and out-of-plane tilt, as shown in Fig. 1(left). The deviation is always shown in mm. Tilts are accomplished by rotation with rotation axes in the centre of the middle VCL. The magnitude of the tilt is taken as the shift of the LFS part of the coil in mm. Therefore, the angle of the tilt is calculated as

$$\alpha = 2 \arcsin \frac{d}{2l} \approx \frac{d}{l}, \tag{7}$$

where l is the length of the rotation arm of the coil and d actual deviation.

The orientation of the misalignments used for the calculations is listed in Table 1. The table also concludes expected values of 3σ for given misalignments. All tilts are calculated with respect to the axis located in the centre of the copper conductor in the TF core, as shown in Fig. 1(left).

3. Current density distribution

Current distribution in the TF coil during the discharge was calculated using a 3D coupled electromagnetic transient, thermal, and structural model in Mechanical APDL software [15]. Small tilts and shifts are assumed not to alter the current diffusion results. The evolution of the current density in a single TF coil is shown in Fig. 2(left). It represents 5 T discharge with ~3 s ramp-up, ~3 s flat-top and ~5 s ramp-down. In the initial phase of the discharge (ramp-up ~70 kA/s), the current peaks in the inner edge of the coil because of the shorter current path at the inner edge of the curved turn and smaller magnetic flux coupled to the inner edge and therefore smaller electromotive force. The current peaking in the initial phase of the discharge results in a hotter inner part of the coil turn and consequently results in higher resistance in the hot region. The current diffuses during the flat-top phase and reaches a mostly uniform distribution. In the final phase, the inner edge has higher resistance and coupling to a smaller magnetic flux, cause that the current starts to peak on the outer edge of the coil. The core part of the TF coil has a wedge-shaped cross-section; therefore, the higher current density in the outer edge of the TF core part does not significantly shift VCL towards the outer edge.

The correct position of the winding layer/virtual current line (VCL) which carries a total TF current of 199.5 kA depends on the TF coil conductor's current distribution and the position used to compute the equivalent current.

Continuous winding of the TF coils results in no increase of TF ripple on HFS as seen on some other machines [4]. The position of equivalent VCL is evaluated for points within the plasma region (various distances from the coil) as shown by the filled region in Fig. 2(right). For the illustration, we show the equivalent VCL position for points in infinity. In the latter, the VCL position equals the centre of mass of the current density distribution. The inner and middle VCL is used in the presented analysis for simplification.

4. Calculated toroidal field ripple on COMPASS-U

Toroidal field ripple without misalignment. First, we analyse the toroidal field ripple of perfectly aligned TF coils as shown in Fig. 3(a). The toroidal field ripple δ increases with a major radius, as is increasing the actual distance between coils. The most significant raise of δ with major radius is observed on the geometrical midplane ($Z = 0$ m). The selected limit of 0.5% is not reached even on the outer first wall when the toroidal field ripple was calculated with current flowing through the middle VCL.

The usage of middle VCL sufficiently represents the steady-state distribution of current in the TF coils. The limit is reached on the separatrix of a typical plasma during flat-top when using current flowing only in the inner VCL. However, this current distribution can be used only in the initial phase of the discharge (as discussed in Section 3) when the plasma either does not yet exist or is small and circular limited on HFS.

Effect of TF coils feeder. The TF coil feeder is located at one of the sixteen TF coils. Although the feeder shape and connection were mostly designed with respect to produced error field and generated joule heat (both topics are not the subject of this article), the contribution to the ripple was also evaluated by the finite element analysis (FEA) model. FEA model consists of the short-circuited feeder, which has a homogeneous current density in the area approximating the steady-state current distribution as close as possible. The magnetic field produced by the feeder and current density is shown in Fig. 4. The feeder mostly increases ripple by decreasing the toroidal magnetic field in the plasma region between TF coils. As a result, the ripple value in the investigated radius is increased by approximately 0.035 pp (percentage point) when the feeder field is considered.

Effect of misalignments

The effect of coil misalignments has been studied using the Monte Carlo (MC) approach, which allows us to evaluate the most probable value of the toroidal field ripple using the mean over the MC runs and the worse expected values using the 99% quantile. Each misalignment was evaluated separately, and the two misalignment types which appeared to have the most significant effect of toroidal field ripple were re-evaluated. For the given value of 3σ, the deviations were taken from the normal (Gaussian) distribution. The effect of the single misalignment type was typically evaluated using 5000 samples randomly taken from the distribution. An example of the resulting distribution of ripple is shown in Fig. 6(b).

All studied misalignments are compared in Fig. 5(a) as the mean value of toroidal field ripple with fixed misalignment distribution of $3\sigma = 2$ mm. With the given error distribution most significant deviations appear to be axis tilt, normal shift and radial shift. In this paper, we will focus on radial shift, and axis tilt as these two misalignments have one of the most significant effects on ripple and mechanically may appear simultaneously. The normal shift will not be further examined since the ripple caused by the normal shift evinces a similar ripple caused by axis tilt. Moreover, the construction of the coils does not allow for the full propagation of both the radial shift and the normal shift misalignment. Fig. 5(b) shows the change of the mean toroidal field ripple on the geometrical midplane with different 3σ for the radial shift. The dependence of the ripple on the 3σ for the two selected misalignments in the centre ($R = 0.7$ m) and on the outer wall ($R = 1.2$ m) is shown in Fig. 5(c, d). Both the mean value and 99% quantile (percentile) are plotted. We can observe an almost linear slope of all watched ripple values within the studied parameters. The mutual interaction of normal shift and radial tilt misalignments can be seen in Fig. 6(a). Due to the computational cost, each data point in this figure was calculated only by 1000 samples.

The spectral analysis of the absolute value of a total magnetic field in a toroidal direction has been performed to understand the

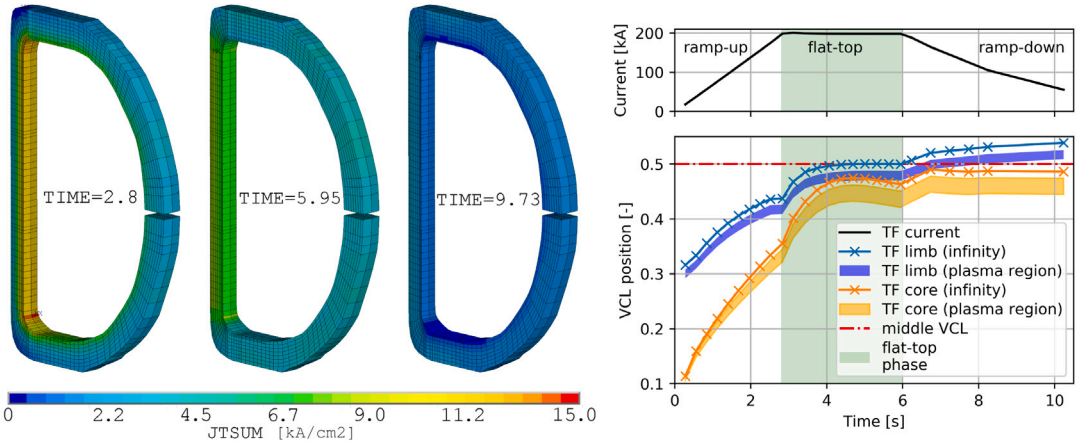

Fig. 2. Current density distribution during ramp-up, flat-top and ramp-down phase of 5 T discharge and its effect on the position of VCL (VCL position = 0 corresponds to inner VCL).

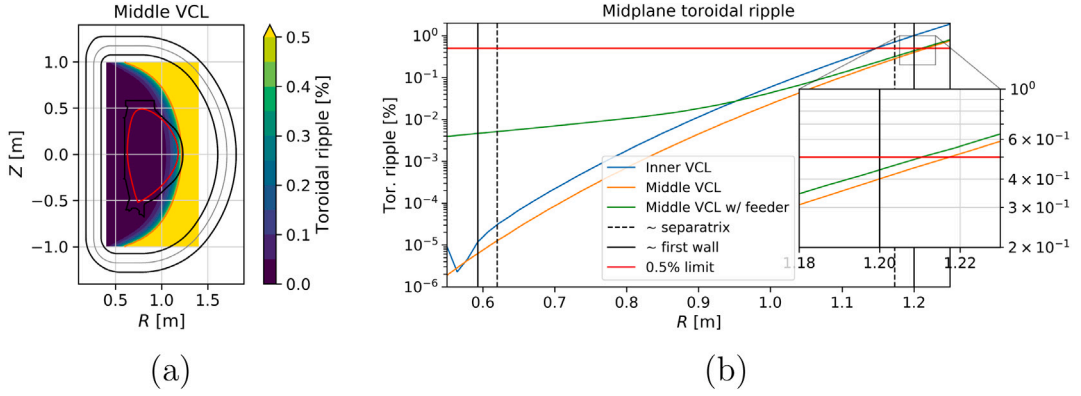

Fig. 3. (a) Toroidal field ripple produced by a perfectly aligned middle VCL of TF coils. The orange line shows the boundary of $\delta = 0.5\%$. (b) Toroidal field ripple is produced by the inner VCL (blue) and by the middle VCL (orange) on the geometrical midplane.

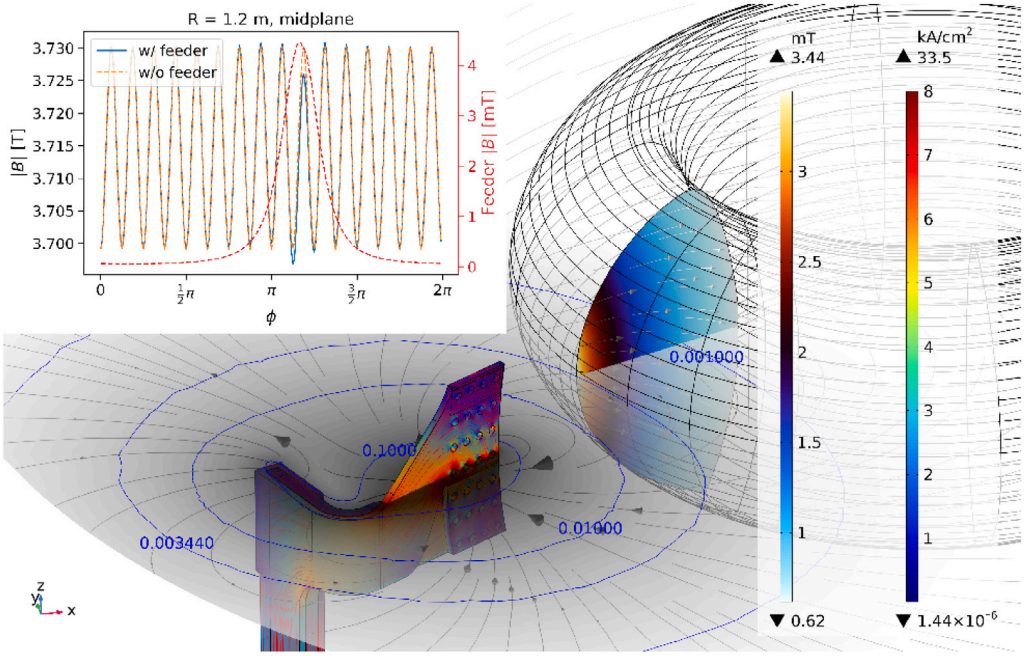

Fig. 4. Feeder stray field represented by streamlines on the midplane and poloidal section between coils. The grey colour at the midplane and magma palette (palette on the left) at the poloidal section represents field magnitude in a logarithmic and linear scale, respectively. Blue contours represent field magnitude. The feeder is coloured by current density and red streamlines. The in-placed graph in the top-left corner shows the absolute value of the magnetic field along the field line with feeder data taken from FEA.

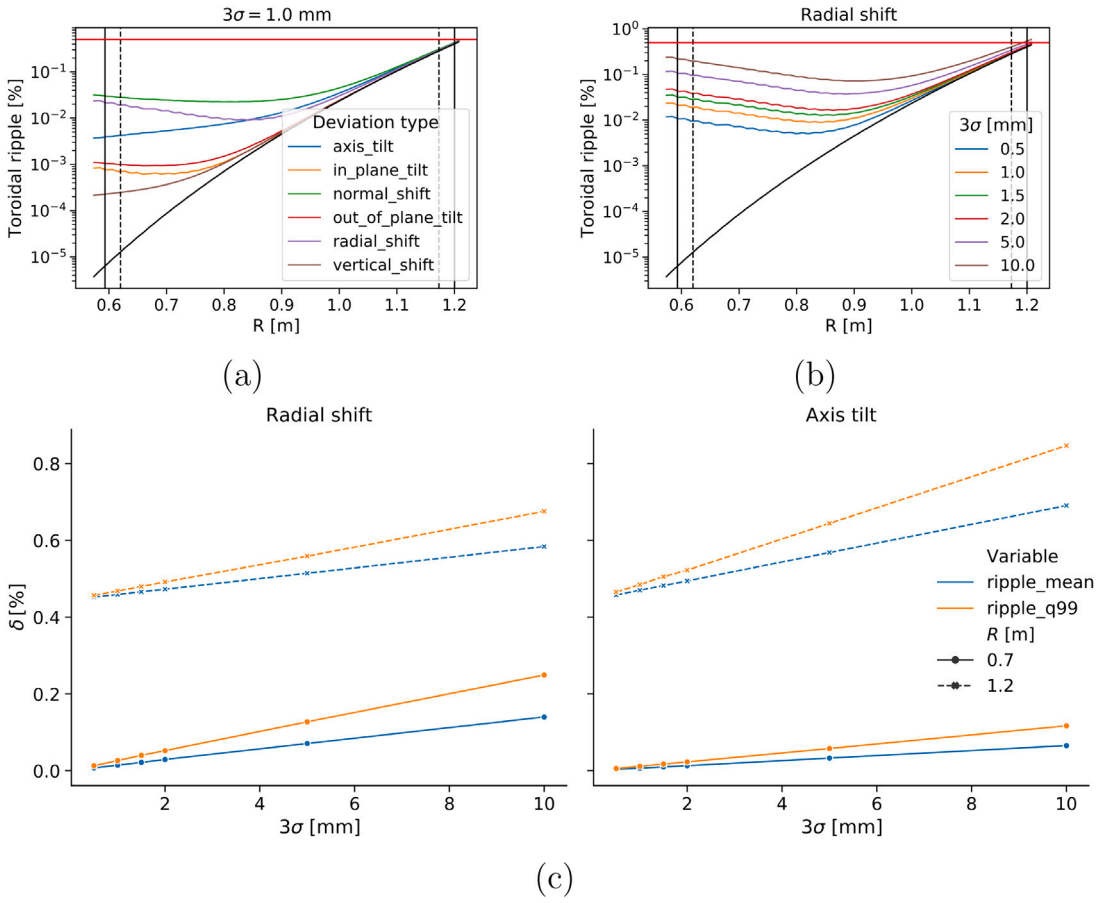

Fig. 5. (a, b) Comparison of mean toroidal field ripple value on the geometrical axis for (a) all evaluated TF coil misalignments for given initial distribution of displacement with $3\sigma = 1$ mm, and (b) for radial displacement with varying value of 3σ. (c) Change of the averaged (and quantile 99%) toroidal field ripple with the change of the initial distribution of misalignment for radial shift and axis tilt displacements.

composition of the ripple. First, Fourier transformation is applied to the magnetic field magnitude of each MC sample and the statistical quantities are consequently calculated from the absolute values of the obtained distribution. As a consequence of the TF coil geometry, the toroidal field ripple is exclusively formed by the $n = 16$ toroidal component of the field perturbation if no misalignment is present. The mean value of Fourier components magnitude (mean$|\mathcal{F}_\phi|\vec{B}(R,Z,\phi)\,\|$) is shown in Fig. 6(c) and (d). The standard deviation of the same quantity (std$|\mathcal{F}_\phi|\vec{B}(R,Z,\phi)\,\|$) has also been plotted and reaches similar values to the mean values. Dominant $n = 0$ Fourier component with value of $\sim 1.7 \times 10^{-2}$ a.u. on the edge (compared to $n = 16$ component with $\sim 3.5 \times 10^{-5}$ a.u.) has been removed in these plots, as well as $n = 16$ in the figure from the low field side (R = 1.2 m) where this perturbation clearly dominates. On the other hand, in the plasma centre, the magnitude of the original $n = 16$ for its dominant perturbation is comparable with perturbation components introduced by misaligned TF coils. Due to the initial Gaussian distribution of the misalignments, the presented graphs represent the most probable composition of the magnetic perturbation. In the central part of the plasma, the magnetic field is most susceptible to $n = 1$–2, while in the edge area of the plasma, one can more probably expect additional ripple with dominant Fourier components of $n = 3$–5, especially in the case of the radial displacement.

To better understand the results, $n = 1$ represents the situation when most of the coils are misaligned on one side; therefore, the field is slightly stronger on that side. The $n = 2$ represents the situation when a specific group of 8 neighbouring coils are slightly misaligned in one direction while the other eight coils are misaligned in the other direction. While this configuration generates pure $n = 1$ or $n = 2$ harmonics, the more likely situation is that a single coil suffers extreme displacement in comparison with other coils and generates $n = 1$ harmonics.

5. Conclusions

ANSYS calculations show that the middle virtual current line can represent toroidal field current distribution for most of the flat-top phase of the COMPASS-U discharge. During the ramp-up phase, the current distribution propagates from the inner to the middle position. Investigation of the current density profile with respect to the used VCL position is not only relevant for bitter-plate-like coils but also for non-insulated HTS coils [16,17].

The goal of toroidal field ripple 0.5% is not exceeded anywhere within the first wall for all considered cases when the middle VCL is used. The analysis shows that the most significant misalignments are normal shift, radial shift and axis tilt. Although normal shift causes slightly higher values of toroidal field ripple in comparison with axis tilt, its magnitude is limited by the presence of the radial shift for construction reasons. The radial shift and axis tilt may appear independently, and the mean ripple in the presence of both misjudgements has been calculated. It is shown that the ripple does not scale as a simple superposition when two types of misalignments are combined. The TF coil feeder contribution to ripple by 0.035 pp (percentage point) at R = 1.2 m is of similar amplitude as ripple caused by misalignment within the evaluated range, which varies by 0.06 pp (percentage point).

The most significant relative effect of misalignments is expected in the centre of the plasma and on the high field side. The mean toroidal field ripple and corresponding 99% quantile scale almost linearly with

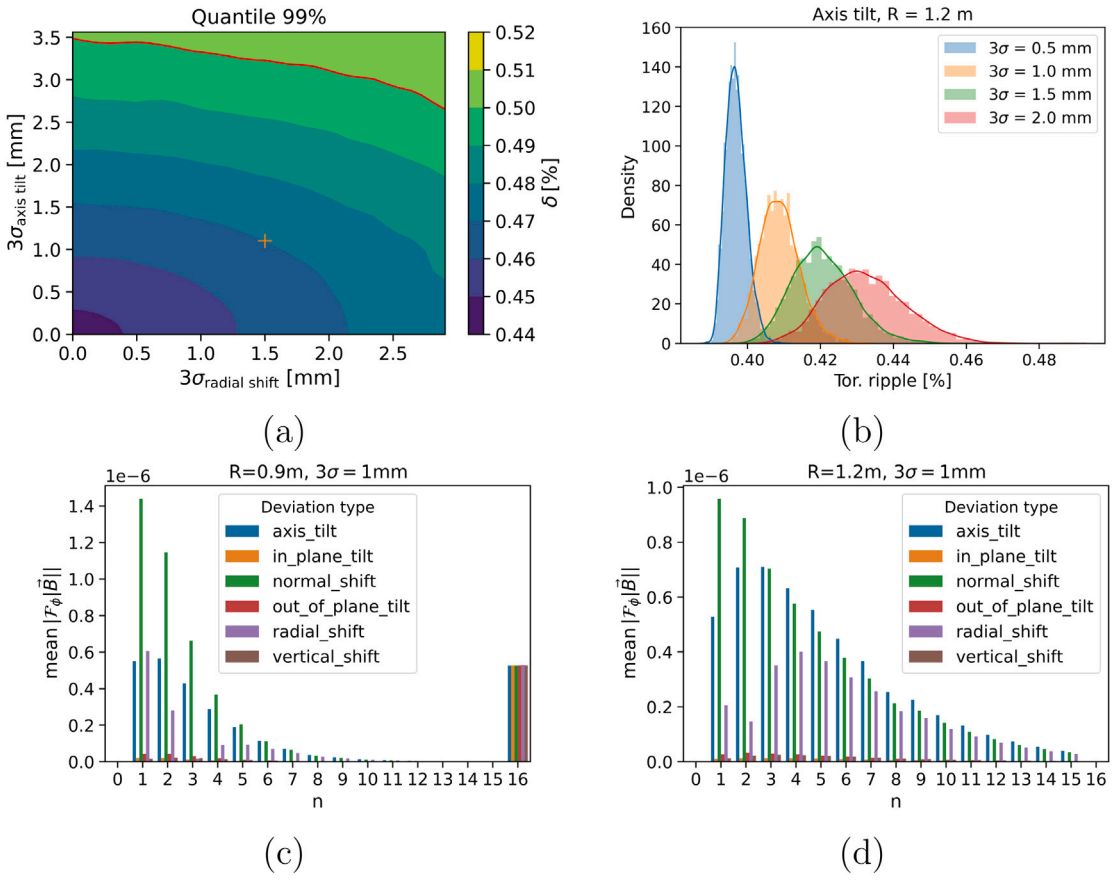

Fig. 6. (a) Mean value of toroidal field ripple when combining axis tilt and radial shift displacements. The expected maximal value of the deviation is marked by the orange plus symbol. (b) Distribution of the toroidal field ripple caused by axis tilt for various initial displacement distributions. (c, d) Mean value over MC iterations of magnitude of Fourier components evaluated at $R = 0.9\,\text{mm}$ (c) and (d) $R = 1.2\,\text{mm}$ on the magnetic midplane. The Fourier transformation is calculated in the toroidal direction from the magnitude of the magnetic field. The $n = 0$ component is removed from both figures (c, d). The $n = 16$ component is removed from the figure (d) for its dominants over other components ($\sim 3.5 \times 10^{-5}$ a.u.).

misalignment distribution width within the tested parameters. The spectral analysis of the magnetic field in the presence of misalignments has been conducted.

CRediT authorship contribution statement

Lukas Kripner: Conceptualization, Methodology, Software, Writing – original draft, Resources, Formal analysis, Data curation, Visualization. **Jaroslav Krbec:** Conceptualization, Methodology, Software, Validation, Formal analysis, Visualization, Writing – original draft, Resources. **Jan Zelda:** Methodology, Resources. **Tomas Markovic:** Methodology, Resources. **Peter Titus:** Software, Resources. **Petr Vondracek:** Supervision, Writing – review & editing. **Ondrej Ficker:** Methodology, Validation. **Martin Hron:** Project administration, Funding acquisition.

Declaration of competing interest

The authors declare that they have no known competing financial interests or personal relationships that could have appeared to influence the work reported in this paper.

Data availability

Data will be made available on request.

Acknowledgements

This work has been carried out within the framework of the project COMPASS-U: Tokamak for cutting-edge fusion research (No. CZ.02.1.01/0.0/0.0/16_019/0000768), co-funded by European structural and investment funds, and Czech Science Foundation project GA19-15229S and by MEYS, Czechia project LM2018117.

References

[1] R. Panek, et al., Conceptual design of the COMPASS upgrade tokamak, Fusion Eng. Des. 123 (2017) 11–156.
[2] p. Vondracek, et al., Preliminary design of the COMPASS upgrade tokamak, Fusion Eng. Des. 169 (2021) 112490.
[3] P.C. de Vries, et al., Effect of toroidal field ripple on plasma rotation in JET, Nucl. Fusion 48 (3) (2008) 035007.
[4] S.D. Scott, et al., Fast-ion physics in SPARC, J. Plasma Phys. 86 (2020) 865860508.
[5] G. Calabro, et al., Toroidal field ripple reduction studies for ITER and FAST, Fusion Eng. Des. 84 (2–6) (2009) 522–525, http://dx.doi.org/10.1016/J.FUSENGDES.2009.01.030.
[6] E. Strumberger, et al., Fast particle losses due to NTMs and magnetic field ripple, New J. Phys. 10 (2) (2008) 023017.
[7] K. Tobita, et al., Ripple induced fast ion loss and related effects in JT-60U, Nucl. Fusion 35 (12) (1995) 1585.
[8] P.J. Catto, Ripple modifications to alpha transport in tokamaks, J. Plasma Phys. 84 (2018) 905840508.
[9] T.E. Stringer, Effect of the magnetic field ripple on diffusion in tokamaks, Nucl. Fusion 12 (1972) 689.
[10] J.W. Connor, R.J. Hastie, Neoclassical diffusion arising from magnetic-field ripples in tokamaks, Nucl. Fusion 13 (1973) 221.

[11] R.J. La Haye, J.T. Scoville, A method to measure poloidal field coil irregularities in toroidal plasma devices, Rev. Sci. Instrum. 62 (9) (1998) 2146, http://dx.doi.org/10.1063/1.1142330.
[12] J. Knaster, et al., ITER non-axisymmetric error fields induced by its magnet system, Fusion Eng. Des. 86 (6–8) (2011) 1053–1056, http://dx.doi.org/10.1016/J.FUSENGDES.2011.02.045.
[13] N.C. Logan, et al., Robustness of the tokamak error field correction tolerance scaling, Plasma Phys. Control. Fusion 62 (8) (2020) 084001, http://dx.doi.org/10.1088/1361-6587/AB9A12.
[14] O. Grover, L. Kripner, Biot–Savart python integrators, https://github.com/smartass101/biot_savart_integrators.
[15] P. Titus, et al., Combined normal and disruption, electromagnetic transient, thermal, and structural analysis of COMPASS upgrade, IEEE Trans. Plasma Sci. 50 (11) (2022) http://dx.doi.org/10.1109/TPS.2022.3182629.
[16] Y. Wang, et al., An equivalent circuit grid model for no-insulation HTS pancake coils, Supercond. Sci. Technol. 28 (4) (2015) 045017.
[17] P.H. Titus, Startup and quench electromagnetic simulation of a bitter plate TF coil concept for the fusion nuclear science facility (FNSF), IEEE Trans. Appl. Supercond. 31 (5) (2021).